

Non-Gaussian properties of global momentum and particle fluxes in a cylindrical laboratory plasma

Yoshihiko Nagashima,^{1,2,a)} Sanae -I. Itoh,^{2,3} Shigeru Inagaki,^{2,3} Hiroyuki Arakawa,⁴ Naohiro Kasuya,^{2,5} Akihide Fujisawa,^{2,3} Kunihiro Kamataki,⁶ Takuma Yamada,^{1,2} Shunjiro Shinohara,⁷ Stella Oldenbürger,² Masatoshi Yagi,^{2,3} Yuichi Takase,¹ Patrick H. Diamond,^{2,8,b)} and Kimitaka Itoh^{2,5}

¹Graduate School of Frontier Sciences, The University of Tokyo, Kashiwa 277-8561, Japan

²Itoh Research Center for Plasma Turbulence, Kyushu University, Kasuga 816-8580, Japan

³Research Institute for Applied Mechanics, Kyushu University, Kasuga 816-8580, Japan

⁴Interdisciplinary Graduate School of Engineering Sciences, Kyushu University, Kasuga 816-8580, Japan

⁵National Institute for Fusion Science, Toki 509-5292, Japan

⁶Center for Research and Advancement in Higher Education, Kyushu University, Fukuoka 816-8580, Japan

⁷Institute of Engineering, Tokyo University of Agriculture and Technology, Koganei 184-8588, Japan

⁸Center for Astrophysics and Space Sciences, University of California San Diego, La Jolla, California 92093, USA

(Received 7 March 2011; accepted 25 May 2011; published online 1 July 2011)

Non-Gaussian statistical properties of the azimuthally averaged momentum and particle fluxes driven by turbulence have been simultaneously observed in inhomogeneous magnetized plasmas for the first time. We identified the stretched Gaussian distribution of the both fluxes and the transition from the point-wise distribution to averaged ones was confirmed. The change of the particle flux precedes that of the momentum flux, demonstrating that the momentum flux is induced by the relaxation of density gradient. © 2011 American Institute of Physics. [doi:10.1063/1.3601767]

Non-Gaussianity of the probability density function (PDF) is one of the key elements that characterize the far-non-equilibrium states.^{1,2} Reports were made on the point-wise measured particle flux in turbulent plasmas,³⁻⁶ where the non-Gaussian PDF of particle flux has often been observed. It was pointed out that even if the local density and electric field perturbation obey the Gaussian statistics, the induced local particle flux can show the exponential tail.⁵ Although progresses have been noticeable in the experimental study of *local* particle flux, measurements of the *global* transport phenomena by turbulence stochasticity are required because relaxation of the far-non-equilibrium media depends upon the global transport of the media. The global momentum flux is essential for the generation of global axial vector field by thermal turbulence (e.g., zonal flow, geo- and astro-dynamo magnetic field, etc).⁷ Furthermore, recent researches have discussed the link between the momentum transport Π and particle transport Γ .⁸ On the whole, *simultaneous* observations of statistics of the global (particle and momentum) transport phenomena are required to understand structural formation in the far-non-equilibrium systems. In this paper, we present the first simultaneous observation of the azimuthally averaged particle and momentum fluxes ($\langle\Gamma\rangle$ and $\langle\Pi\rangle$, respectively) by turbulence in inhomogeneous cylindrical magnetized plasmas. Statistical properties of the both fluxes were investigated in detail, and we found that both $\langle\Pi\rangle$ and $\langle\Gamma\rangle$ obey the stretched Gaussian distribution, $P(X) \propto \exp(-c_X X^{\alpha_X})$ where $X = \langle\Pi\rangle$ or $\langle\Gamma\rangle$, and the indices $\alpha_{\langle\Pi\rangle}$ and $\alpha_{\langle\Gamma\rangle}$ were obtained. The transition

from the point-wise index to averaged ones is identified. The simultaneous observation of the two fluxes realizes the joint PDF of the two fluxes as well as correlation analysis between the both fluxes. The change of $\langle\Gamma\rangle$ precedes that of $\langle\Pi\rangle$, demonstrating that the momentum flux is induced by the relaxation of density gradient.

Fully-developed drift-wave turbulence in a linear device (the Large Mirror Device-Upgrade, LMD-U (Ref. 9)) is studied. Magnetic field strength B is fixed at 0.09 T in the center of the vessel, and the ion cyclotron frequency f_{ci} is ~ 34 kHz. Auto-power spectra of the ion saturation current $I_{i,sat}$ and floating potential Φ_f fluctuations have broadband property¹⁰ combined with some spectral peaks observed at ~ 1 kHz ($f/f_{ci} \sim 0.03$, $m \sim -1$) and ~ 4 and 7-8 kHz ($f/f_{ci} \sim 0.12$, 0.22 and $m \sim 0-1$, 2), shown in Fig. 1(a). Two types of the probe array were used in this experiment to compare the two flux quantities, the Π and Γ , at the same radial location $r = 4$ cm where the local momentum transport has a maximum (Fig. 1(b)). (Radius of the cylindrical plasma is 5 cm.) Our main interest is the origin of the momentum flux, therefore, we chose the radius $r = 4$ cm as the observation location here. The Π was measured with 16 channel Reynolds stress probe array (16ch-RSP).¹¹ The 16ch-RSP is arranged approximately at regular intervals in the azimuthal direction. The Γ was simultaneously measured with the 64ch azimuthal probe array.¹² (The $I_{i,sat}$ and Φ_f were measured alternately along the azimuthal direction to observe the particle flux.) The two probe arrays are located at the same radial location within the accuracy of 1 mm. We compute the stationary Φ_{fs} averaged azimuthally and temporally with the 16ch-RSP ($\langle\langle\Phi_{f,RSP}\rangle\rangle$) and with the 64ch azimuthal probe array ($\langle\langle\Phi_{f,64ch}\rangle\rangle$), and the accuracy $\delta = 1$ mm was obtained from

^{a)}Author to whom correspondence should be addressed. Electronic mail: nagashima@k.u-tokyo.ac.jp.

^{b)}Also at WCI Center for Fusion Theory, National Fusion Research Institute, Yuseong-Gu 305-333, South Korea.

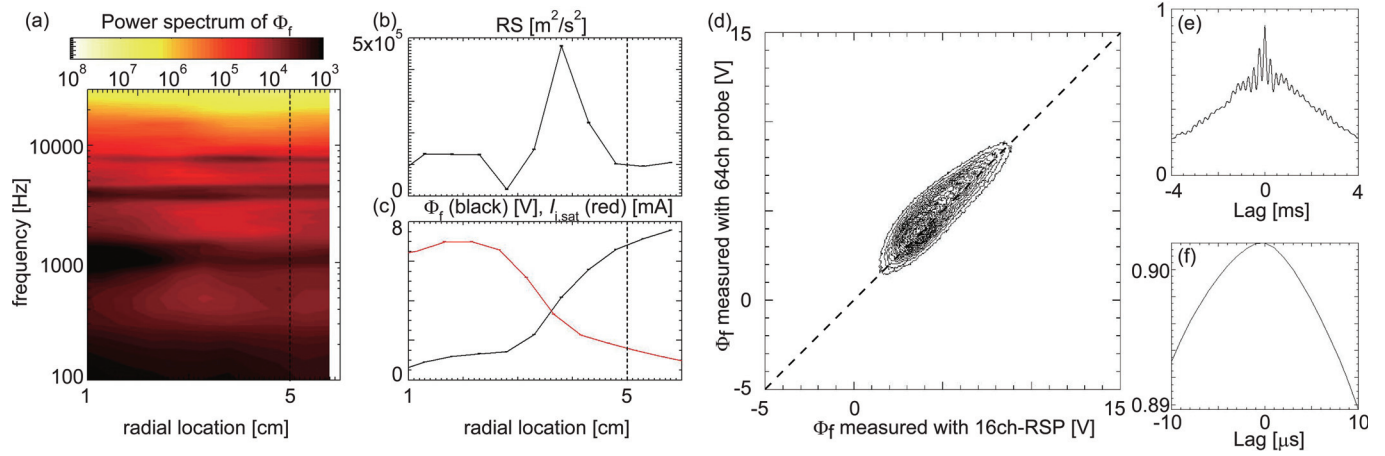


FIG. 1. (Color) (a) Radial profile of auto-power spectrum of floating potential. Radial profiles of (b) point-wise turbulence momentum flux and (c) time-averaged floating potential (black) and ion saturation current (red). (d) Joint PDF between the floating potential measured with the RSP and the one measured with the 64ch probe. (e) and (f) Normalized cross-correlation functions between azimuthally averaged floating potentials measured with RSP and those measured with the 64ch probe. The complete range of (f) is the same as for (e), but the plotted range is restricted to $\pm 10 \mu\text{s}$.

the expression $\frac{\partial \overline{\Phi_f}}{\partial r} \delta = \overline{\langle \Phi_f \rangle_{\text{RSP}}} - \overline{\langle \Phi_f \rangle_{\text{64ch}}}$. Here, for the physical quantity X , \bar{X} indicates temporal average over time scale much longer than $f_{\text{fluctuation}}^{-1}$. Average $I_{i,\text{sat}}$ and Φ_f have radial gradient, shown in Fig. 1(c), and they demonstrate that the target plasma is under the far-non-equilibrium state. Turbulent fluxes are mainly driven by fluctuations at the frequency range less than 10 kHz. For instance, the values of the mean turbulent fluxes are $\overline{\langle \Gamma \rangle}_{f < 30 \text{ kHz}} \sim 1.12 \times 10^{20} \text{ m}^{-2} \text{ s}^{-1}$, $\overline{\langle \Gamma \rangle}_{f < 10 \text{ kHz}} \sim 1.07 \times 10^{20} \text{ m}^{-2} \text{ s}^{-1}$, $\overline{\langle \Pi \rangle}_{f < 30 \text{ kHz}} \sim 3.38 \times 10^5 \text{ m}^2 \text{ s}^{-2}$, and $\overline{\langle \Pi \rangle}_{f < 10 \text{ kHz}} \sim 3.03 \times 10^5 \text{ m}^2 \text{ s}^{-2}$.

In this experiment, the Γ and Π are observed with two diagnostics located axially 25 cm from each other. The axial phase difference of fluctuations may affect the comparison between the Γ and Π . To validate the comparison, the joint PDF of $\langle \Phi_f \rangle$ observed with the two diagnostics is shown in Fig. 1(d). Good correlation is found between the $\langle \Phi_f \rangle$ s measured with the two arrays. The normalized cross-correlation functions between the azimuthally averaged floating potential measured with the RSP and the one measured with the 64ch probe were also investigated, as shown in Figs. 1(e) and 1(f). The stationary components are subtracted before the analysis. The maximum correlation larger than 0.9 implies that axial decay of turbulence correlation between the $\langle \Phi_f \rangle$ s measured with the two probe arrays is negligible. In addition, the time lags at the maximum correlation are smaller than 1 μs (the sampling time step = 1 μs), and this implies that the axial phase shift is also negligibly small. Therefore, we compare the two flux quantities measured with the two probe arrays under the hypothesis that the turbulence, which is analyzed here, is quasi-two-dimensional.

PDFs of plasma fluctuations have been intensively investigated to clarify statistics of transport events. Non-Gaussian properties of Γ and Π have been studied theoretically^{5,13,14} and experimentally.^{4-6,15-17} Global transport phenomena are determined by the flux events averaged over the flux surface and/or over the full azimuthal direction. To show the evidence

of the difference of PDFs between the local one and azimuthally-averaged one, dependence of PDF of azimuthally averaged Reynolds stress (RS) on the number of the RSP is first shown. We compute $\Pi(t:N) = \left(\sum_{j=1}^N \Pi_j(t) \right) / N$, where $\Pi_j(t)$ is the flux which is measured by the j -th probe in 16 consecutive probes. (Here, N is the number of consecutive probes, over which averaging is taken.) The PDF of $\Pi(t:N)$ is measured and shown in Fig. 2(a). As summation number N increases, the statistical properties of PDF (i.e., mean, standard deviation, skewness, and kurtosis) proceed to converging on finite values ($N=8-16$). Non-Gaussian, non-diffusive transport dominates in the observed drift-wave turbulence.

Non-Gaussian PDFs of fluxes are characterized by their tail forms. Figure 3(a) shows calculated tail exponent of the PDF of the $\langle \Pi \rangle$. Least square fittings are performed, and $\alpha = 1.208$ is obtained. The $P(\Pi)$ covers three or four orders of magnitude, and therefore, the exponent can be precisely determined. We show here that, in a turbulent plasma, the PDFs of flux follow the stretched Gaussian law (different from the Gaussian, shown in Fig. 3(b)). The stretched Gaussian distribution is defined as $P(X) \propto \exp(-c_X X^{2\alpha})$ where $X = \langle \Pi \rangle$ or $\langle \Gamma \rangle$, and the indices $\alpha_{\langle \Pi \rangle}$ and $\alpha_{\langle \Gamma \rangle}$ were obtained. We next analyze the relation between the point-wise RS and the RS which is summed over the azimuthal direction. For this purpose, the dependence of the tail exponent α of the RS PDF on the summation number N is studied. We found that the tail of PDF of $\Pi(t:N)$ is fitted to the stretched Gaussian distribution as well (Figure 3(a)). For $\langle \Pi \rangle$, we observed that the exponent varies from 0.6 (point-wise) to 1.2 (averaged), as the spatial length of averaging becomes longer and converges to a constant value. For $\langle \Gamma \rangle$, we have $\alpha \sim 1.75$ with $N = 16$.

The origin of the difference between the local PDF and the spatially averaged PDF is the internal structure of the turbulence flux event. The PDF of point-wise flux represents “microscopic” dynamics. The averaging over spatial range larger than that of the flux event causes mixing among the different flux events; here, averaged flux quantity converges. The azimuthal size of the flux event is smaller than the arc-

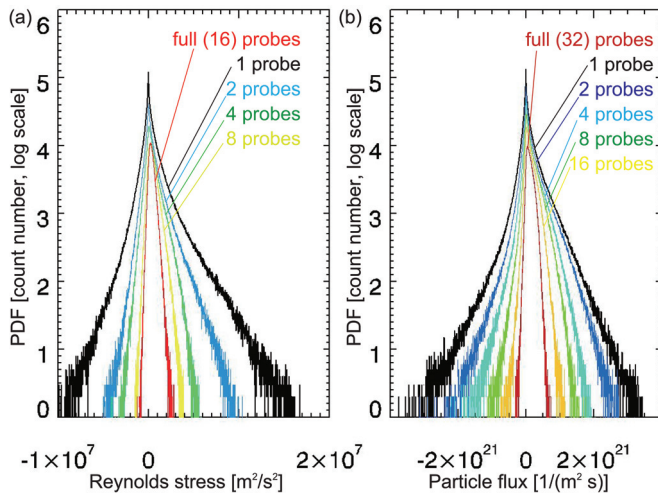


FIG. 2. (Color) Dependence of PDFs of (a) the turbulence momentum flux and (b) the turbulence particle flux on summation number of probes. Difference of colors indicates difference of numbers of probes used in averaging over the azimuthal direction. Significant difference between point-wise PDFs and azimuthally averaged ones is confirmed.

length shared by 4 RSPs, which is the characteristic wavelength of dominant modes in turbulence. Figure 3(c) clearly demonstrates that the mixing of these microscopic dynamics constitutes the PDF for the azimuthally-averaged flux.

In order to clarify the causal relationship between the two flux events (i.e., $\langle \Gamma \rangle$ and $\langle \Pi \rangle$), the time lags between $\langle \Gamma \rangle$ and $\langle \Pi \rangle$ are evaluated by the use of the cross-correlation technique. Figure 4 shows histograms of time lags between $\langle \Gamma \rangle$ and $\langle \Pi \rangle$. About 28 000 data windows from 14 shots are used to obtain the data of delay time at the maximum correlation. Cross-correlations between $\langle \Gamma \rangle$ and $\langle \Pi \rangle$ are found to be typically around 0.4–0.45; thus, phase relation is credible, although there is a large variance in the time-lag. Fluctuation frequency ranges were chosen as 1–10 kHz and 1–30 kHz in digital filtering. Histograms differ for the two frequency ranges. For the 1–30 kHz data, a significant peak appears at $\sim -25 \mu\text{s}$ with a

secondary one at $\sim 25 \mu\text{s}$. The peak at negative time lag indicates that $\langle \Gamma \rangle$ leads $\langle \Pi \rangle$. For the 1–10 kHz data, the histogram has a significant peak at $-25 \mu\text{s}$. In both cases, probability at the lag time of $\sim -25 \mu\text{s}$ is the largest, indicating that the $\langle \Gamma \rangle$ mainly leads $\langle \Pi \rangle$ by $\sim 25 \mu\text{s}$. For two-dimensional turbulence, the measurement of time lag is not affected by the difference of measurement locations between the $\langle \Gamma \rangle$ and $\langle \Pi \rangle$. Long-time averages of fluxes are sustained by fluctuations in the frequency range of 1–10 kHz as is explained in the beginning of this article. The observation of the significant peak at $-25 \mu\text{s}$ in Fig. 4 demonstrates the causal relationship between the particle flux and the momentum flux in this plasma turbulence. We have confirmed that the change of $\langle \Gamma \rangle$ precedes that of $\langle \Pi \rangle$, demonstrating that the momentum flux is induced by the relaxation of density gradient.

The joint PDF technique is a powerful tool to clarify the correlation between two turbulent quantities. The joint PDF is constructed for the pair of variables $P(\langle \Gamma(t) \rangle, \langle \Pi(t + 25 \mu\text{s}) \rangle)$ and is shown in Fig. 5. The contour of joint PDF has a “pearl shell” shape. In the contour plots, positive $\langle \Gamma \rangle$ is mainly correlated with positive $\langle \Pi \rangle$ and this confirms the significant correlation between $\langle \Gamma \rangle$ and $\langle \Pi \rangle$ in the tail parts. In addition, the variance in the joint PDF must also be highlighted. The Reynolds stress has a large variance for a given value of the particle flux, even in the tail of PDF. This indicates that the deviation of $\langle \Pi \rangle$ from long-time mean of $\langle \Pi \rangle$, $\overline{\langle \Pi \rangle}$, remains substantially, both for the bulk and tail of the distribution of $\langle \Gamma \rangle$. The deviation from the mean distribution is the key that characterizes the dynamical property of non-equilibrium media as is illustrated in Ref. 18. The quantities $\nabla \cdot (\langle \Pi \rangle - \overline{\langle \Pi \rangle})$ and $\nabla \cdot (\langle \Gamma \rangle - \overline{\langle \Gamma \rangle})$ are interpreted as fluctuating stress and fluctuating source, respectively, in the transport equations for mean profiles. The general importance of such fluctuation parts is stressed in modern plasma physics.¹⁹ An example of their impacts is seen in the onset of transition in plasma confinement. Collisional damping force for rotation in toroidal plasmas becomes a decreasing function of the rotation velocity

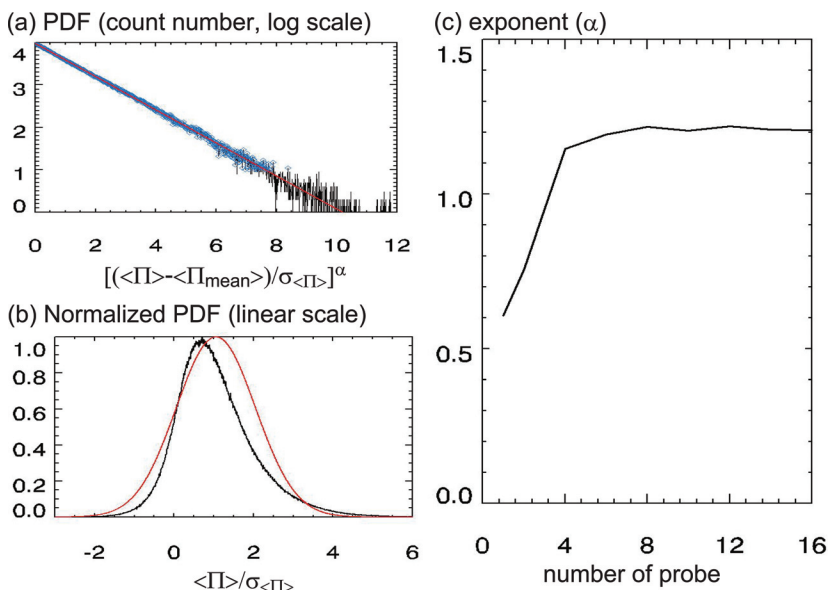


FIG. 3. (Color) (a) Logarithm plot of azimuthally averaged positive PDF of RS ($\langle \Pi \rangle$) vs. $(\langle \Pi \rangle - \langle \Pi_{\text{mean}} \rangle)^2$. Black points are full PDF data, blue squares are data used to determine the most likely value of α , and red line indicates PDF with the most likely value of α . An α value of 1.208 is obtained as a result of the least square fitting, thus, the PDF of RS is far from Gaussian feature. (b) PDF of the Reynolds stress (black) and Gaussian distribution function (red) with mean and variance same as those of the Reynolds stress PDF. (c) Dependence of tail exponents of the PDF of the RS upon number of contiguous RSPs summed sequentially in the azimuthal direction in estimation of the tail exponents. The tail exponents start to converge when the number of probes used in averaging is larger than 4. PDFs of the global transport are non-Gaussian.

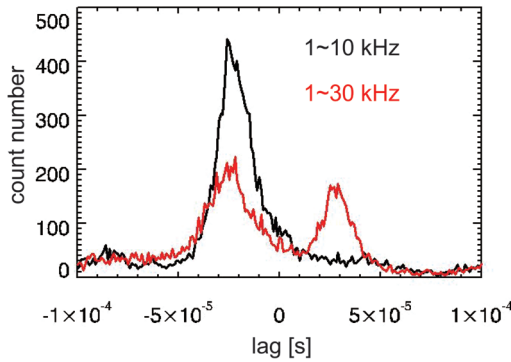


FIG. 4. (Color) Histograms of time lags at the maximum correlation between azimuthally averaged Reynolds stress per mass density ($\langle \Pi \rangle$) and azimuthally averaged radial particle flux ($\langle \Gamma \rangle$). From about 28 000 data windows. Distributions of time lag are obtained from the time series data of 1–10 kHz (black) and from the data of 1–30 kHz (red). In both cases, probability at the lag time of $\sim -25 \mu\text{s}$ is the largest. The $\langle \Gamma \rangle$ mainly leads $\langle \Pi \rangle$ by $\sim 25 \mu\text{s}$.

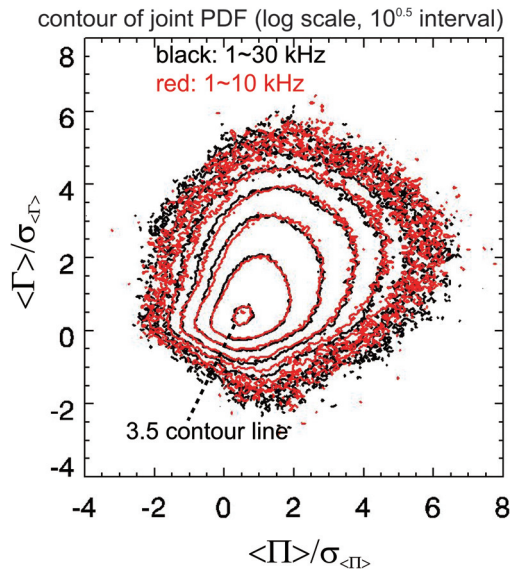


FIG. 5. (Color) Logarithm contour of joint PDFs of azimuthally averaged Reynolds stress per mass density ($\langle \Pi \rangle$) and azimuthally averaged radial particle flux ($\langle \Gamma \rangle$). Contours are plotted at 0.5 intervals. Horizontal or vertical axis indicates $\langle \Pi \rangle$ or $\langle \Gamma \rangle$ normalized by their respective standard deviation. Joint PDF in the frequency range 1–30 kHz is plotted in black, and that in the 1–10 kHz range is plotted in red. Time series of $\langle \Gamma \rangle$ are delayed by $25 \mu\text{s}$ relative to those of $\langle \Pi \rangle$, so that the plot for a perfect correlation would correspond to a straight line through the origin. The PDFs of $\langle \Pi \rangle$ are correlated with those of $\langle \Gamma \rangle$, but the variance between them is also significant.

above a certain threshold.¹⁸ Thus, the transition to the state of higher rotation velocity shear is strongly enhanced by the presence of fluctuating force and source.²⁰ The finding of the variance in the joint PDF indicates that the fluctuating force and fluctuating source must be introduced as independent terms for constructing the dynamical equation of mean parameters of plasmas far from equilibrium.

The observation of the indices α_X ($X = \Pi, \langle \Pi \rangle, \Gamma, \langle \Gamma \rangle$) is compared to theoretical considerations. With the assumption of Gaussian fluctuation fields, the PDF of point-wise Γ is predicted to have an exponential tail (i.e., $\alpha_\Gamma = 1$),⁵ while that of Π was shown to be a stretched Gaussian with $\alpha_\Pi = 1.5$.¹³ Analysis of the flux-averaged particle flux $\langle \Gamma \rangle$ in

simulation has suggested a log-normal or extreme value distribution (EVD, Ref. 14) or stretched Gaussian distribution.²² Importance of studying PDF of the global fluxes has been recognized, e.g., in conjunction with the possible avalanche in particle flux²¹ or in understanding the fluctuating momentum flux (i.e., noise force) on the generation processes of the global fields. The relation between the non-Gaussian property of fluctuating fields and that of particle/momentum fluxes will be discussed in future article.

This work was partly supported by Grant-in-Aid for Specially-Promoted Research (16002500) of MEXT Japan, by Grants-in-Aid for Young Scientist (B) (18760637) and for Scientific Research (21224014, 19360148) of JSPS Japan, by the collaboration programs of NIFS (NIFS07KOAP017, NIFS10KOAP023), of the RIAM of Kyushu University and of the University of Tokyo, and by Asada Eiichi Science foundation. Two of the authors (S.I.I. and K.I.) acknowledge discussion with Professor H. Mori and Dr. V. Naulin.

¹G. M. Zaslavsky, *Hamiltonian Chaos and Fractional Dynamics* (Oxford University Press, Oxford, 2005).

²R. Metzler and J. Klafter, *Phys. Rep.* **339**, 1 (2000).

³T. Huld, S. Iizuka, H. L. Pecseli, and J. J. Rasmussen, *Plasma Phys. Controlled Fusion* **30**, 1297 (1988).

⁴M. Endler, H. Niedermeyer, L. Giannone, E. Kolzhauer, A. Rudyj, G. Theimer, and N. Tsois, *Nucl. Fusion* **35**, 1307 (1995).

⁵B. A. Carreras, C. Hidalgo, E. Sánchez, M. A. Pedrosa, R. Balbín, I. García-Cortés, B. van Milligen, D. E. Newman, and V. E. Lynch, *Phys. Plasmas* **3**, 2664 (1996).

⁶C. Hidalgo, B. Gonçalves, M. A. Pedrosa, J. Castellano, K. Erents, A. L. Fraguas, M. Hron, J. A. Jiménez, G. F. Matthews, B. van Milligen, and C. Silva, *Plasma Phys. Controlled Fusion* **44**, 1557 (2002).

⁷P. H. Diamond, S.-I. Itoh, K. Itoh, and T. S. Hahm, *Plasma Phys. Controlled Fusion* **47**, R35 (2005).

⁸P. H. Diamond, C. J. McDevitt, Ö. D. Gürcan, T. S. Hahm, W. X. Wang, E. S. Yoon, I. Holod, Z. Lin, V. Naulin, and R. Singh, *Nucl. Fusion* **49**, 045002 (2009).

⁹K. Terasaka, S. Shinohara, Y. Nagashima, T. Yamada, M. Kawaguchi, T. Maruta, S. Inagaki, Y. Kawai, N. Kasuya, M. Yagi, A. Fujisawa, K. Itoh, and S.-I. Itoh, *J. Plasma Fusion Res.* **2**, 31 (2007).

¹⁰H. Arakawa, S. Inagaki, Y. Nagashima, T. Yamada, K. Kamataki, T. Kobayashi, S. Sugita, M. Yagi, N. Kasuya, A. Fujisawa, S.-I. Itoh, and K. Itoh, *Plasma Phys. Controlled Fusion* **52**, 105009 (2010).

¹¹Y. Nagashima, S. Inagaki, K. Kamakaki, H. Arakawa, T. Yamada, S. Shinohara, Y. Kawai, M. Yagi, A. Fujisawa, S.-I. Itoh, K. Itoh, and Y. Takase, *Rev. Sci. Instrum.* **82**, 033503 (2011).

¹²T. Yamada, Y. Nagashima, S. Inagaki, Y. Kawai, M. Yagi, S.-I. Itoh, T. Maruta, S. Shinohara, K. Terasaka, M. Kawaguchi, M. Fukao, A. Fujisawa, and K. Itoh, *Rev. Sci. Instrum.* **78**, 123501 (2007).

¹³E. J. Kim and P. H. Diamond, *Phys. Rev. Lett.* **88**, 225002 (2002).

¹⁴V. Naulin, O. E. García, A. H. Nielsen, and J. J. Rasmussen, *Phys. Lett. A* **321**, 355 (2004).

¹⁵C. Hidalgo, B. Gonçalves, C. Silva, M. A. Pedrosa, K. Erents, M. Hron, and G. F. Matthews, *Phys. Rev. Lett.* **91**, 065001 (2003).

¹⁶Z. Yan, J. H. Yu, C. Holland, M. Xu, S. H. Müller, and G. R. Tynan, *Phys. Plasmas* **15**, 092309 (2008).

¹⁷M. Ramisch, G. Birkenmeier, T. Happel, A. Köhn, N. Mahdizadeh, P. Manz, B. Nold, R. Wilcox, D. T. Anderson, and U. Stroth, *Contrib. Plasma Phys.* **50**, 718 (2010).

¹⁸A. Yoshizawa, S.-I. Itoh, and K. Itoh, *Plasma and Fluid Turbulence: Theory and Modelling* (Institute of Physics Publishing, Bristol and Philadelphia, 2002).

¹⁹P. H. Diamond, S.-I. Itoh, and K. Itoh, *Modern Plasma Physics: Volume 1, Physical Kinetics of Turbulent Plasmas* (Cambridge University Press, New York, 2010).

²⁰S.-I. Itoh and K. Itoh, *J. Phys. Soc. Jpn.* **69**, 427 (2000).

²¹B. A. Carreras, D. Newman, V. E. Lynch, and P. H. Diamond, *Phys. Plasmas* **3**, 2903 (1996).

²²S. Sugita, M. Yagi, S.-I. Itoh, and K. Itoh, *J. Phys. Soc. Jpn.* **79**, 044502 (2010).